Application of a distinctly bent, trinuclear, end-to-end azide bridged, mixed valence cobalt(III/II/III) complex in the fabrication of photosensitive Schottky barrier diode

Sudip Bhunia,[a] Mainak Das,[b] Snehasis Banerjee,[c] Michael. G. B. Drew,[d] Partha Pratim Ray[b],* and Shouvik Chattopadhyay[a],*

[a]*Department of Chemistry, Inorganic Section, Jadavpur University, Kolkata 700032, India. E-mail: shouvik.chattopadhyay@jadavpuruniversity.in; shouvik.chem@gmail.com; Tel: +91 3324572941*

[b]*Department of Physics, Jadavpur University, Kolkata 700032, India. E-mail: parthap.ray@jadavpuruniversity.in; Fax: +91 3324138917*

[c]*Department of Higher Education, (University Branch) Government of West Bengal, Bikash Bhavan, Salt Lake, Kolkata-91, India.*

[d]*School of Chemistry, The University of Reading, P. O. Box 224, Whiteknights, Reading RG6 6AD, UK*

Physical measurement

Elemental analyses (carbon, hydrogen and nitrogen) were performed using a Perkin-Elmer 240C elemental analyzer. A Perkin-Elmer RX-1 FTIR spectrophotometer was used to record the IR spectra in the range of 4500–500 cm^{-1} for KBr. Electronic spectra in acetonitrile were recorded on UV-Vis-spectrofluorometer, SHIMADZU (UV-1900i). The magnetic susceptibility measurements were done with an EG&PAR vibrating sample magnetometer,

model 155 at room temperature and diamagnetic corrections were made using Pascal's constants. Effective magnetic moments were calculated using the formula $\mu_{eff} = 2.828(\chi_M T)^{1/2}$, where χ_M is the corrected molar susceptibility. Cyclic voltammetry was carried out using a Metrohm Autolab electrochemical analyzer in a potential range from -2.0 V to +2.0 V with a scan rate of 200 mVs^{-1} using glassy carbon as working electrode, Ag/AgCl as reference electrode and platinum wire as auxiliary electrode at ambient temperature (300 K) under argon (Ar) atmosphere. Electro-spray ionization mass spectrum of the complexwas recorded on Waters Xevo G2 Q-TOF.

X-Ray crystallography

A suitable single crystal was chosen, and mounted on a glass fibre. Reflection data were collected with a 'Bruker D8 QUEST area detector' diffractometer equipped with graphite-monochromated Mo-K$_\alpha$ radiation (λ = 0.71073 Å). The SHELXT-program [S1]was used to directly solve the chemical structure and it was then refined .using full-matrix least squares on F^2 with the SHELXL16-6 program. Different Fourier maps were used to find the hydrogen atoms bound to the oxygen atoms and to maintain their fixed positions. Anisotropic thermal parameters were refined for non-hydrogen atoms. All other hydrogen atoms were placed in their geometrically idealized positions and constrained to ride on their parent atoms. Using the SADABS[S2] programme, multi-scan absorption adjustments were performed to the data. The final difference Fourier map showed several weak peaks indicative of disordered solvent molecules. We therefore used SQUEEZE which identified electron density indicative of one molecule of methanol per asymmetric unit.

The quality of the crystal was less than ideal and as a result the diffraction data were poor as indicated by plots of I/σ(I) vs. resolution which showed the weakness of the data and

R_{merge} vs. resolution plots which showed the unreasonably high Rint value (Figures S1 and S2). .The scan width and exposure time are 0.5° and 2 sec, respectively
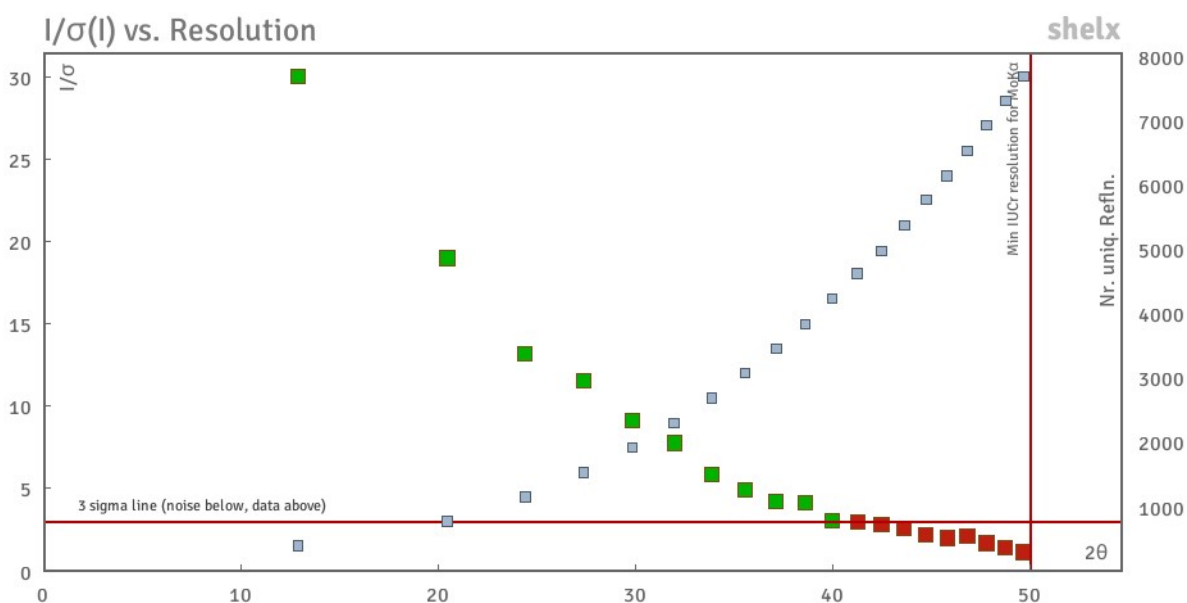

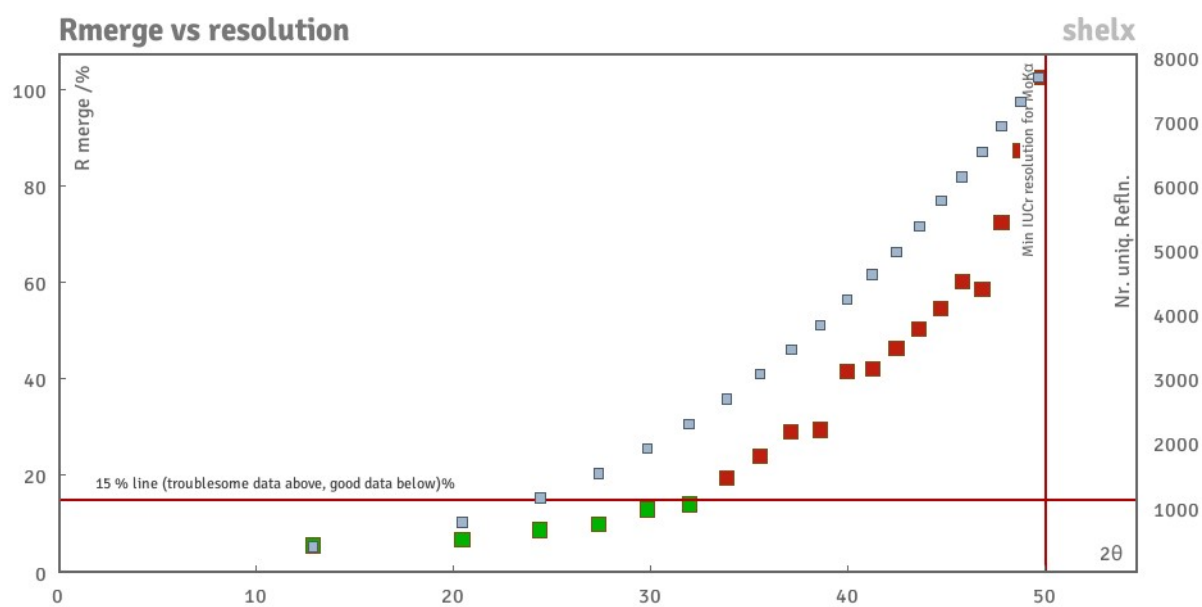**Fig. S1:**$I/\sigma(I)$ vs. resolution plot

Figure S2: R_{merge} vs. resolution plot

Hirshfeld surface analysis

Crystal Explorer[S3] has been used to calculate Hirshfeld surfaces[S4-S6] and the corresponding two-dimensional (2D) fingerprint[S7-S9] plots, with bond lengths to hydrogen atoms set to standard values.[S10] On the Hirshfeld surface, two distances, d_e and d_i, are specified for each point. Here, d_e is the distance from the point to the nearest nucleus external to the surface and d_i is the distance to the nearest nucleus internal to the surface. The normalized contact distance (d_{norm}) based on d_e and d_i is defined as follows:

$$d_{norm} = \frac{(d_i - r_i^{vdw})}{r_i^{vdw}} + \frac{(d_e - r_e^{vdw})}{r_e^{vdw}}$$

Where, r_i^{vdw} and r_e^{vdw} are the van der waals radii of the atoms. Depending on whether intermolecular interactions are shorter or longer than van der Waals separations, the value of d_{norm} may be negative or positive. The parameter d_{norm} shows a surface with a red-white-blue colour to display intermolecular contacts. The red spots on the Hirshfeld map indicate shorter contacts, white spots denote the contacts around the van der Waals separation and blue spots are for larger contacts. The interactions in the crystal are succinctly summarised by 2D-fingerprint displays. For a fixed CIF, the Hirshfeld surface is exclusive.[S11]

The Hirshfeld surfaces are mapped over d_{norm} (range −0.1 Å to 1.5 Å), shape index and curvedness (Fig. S3). Red spots on the Hirshfeld surfaces mapped with d_{norm} denote the dominant interactions. Shape index can be used to identify complementary red hollows and blue bumps, where two molecular surfaces touch one another. Curvedness is a function of the r.m.s. curvature of the surface. Relatively flat areas in the maps of curvedness are typically shown large regions of green and the areas with large positive curvature are represented by dark blue edges.
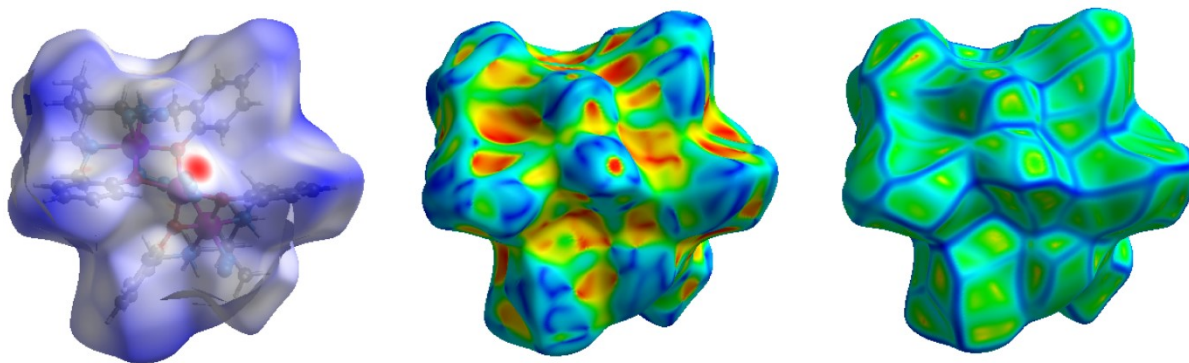
Fig. S3 Hirshfeld surfaces of the complex mapped with d_{norm} (left), shape index (middle) and curvedness (right).

The intermolecular interactions appear as distinct spikes in the 2D fingerprint plot shows the different spikes with their corresponding interactions. The visible spots in Hirshfeld surface of the complex correspond to H···H (58.4%), C···H/H···C (11.1%) and N···H/H···N (21.8%) contacts. 2D fingerprint plot of the complex is shown in Fig. S4.
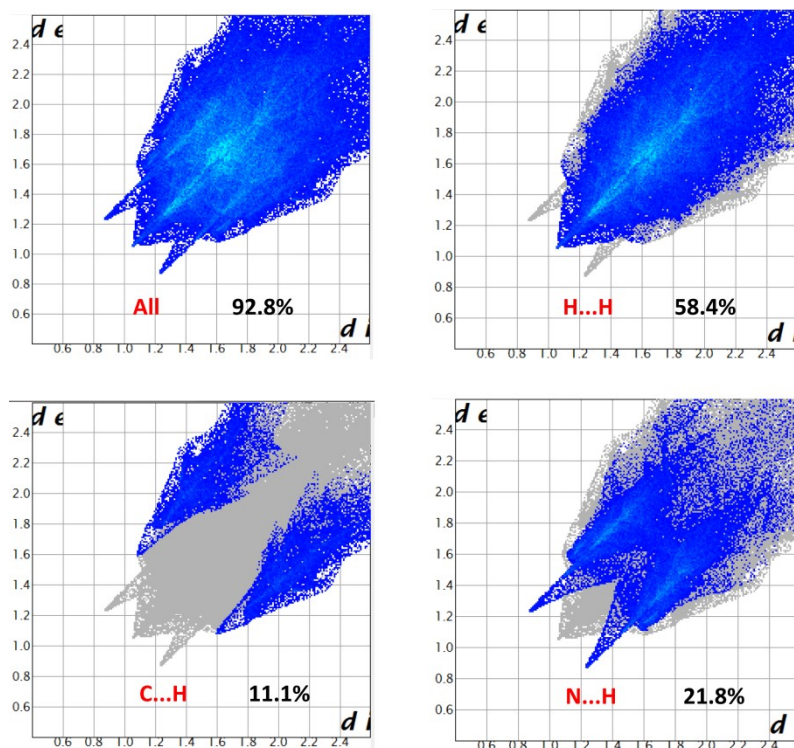
Fig. S4 Fingerprint plot of the complex: Full and resolved into H···H, C···H/H···C and N···H/H···N contacts contributed to the total Hirshfeld Surface area.

Noncovalent Interactions

The following discussion relies on single-point calculations for the hydrogen (H) atom-optimized X-ray diffraction (XRD) geometries of our systems, specifically without full optimization. This choice is attributed to the fact that crystal packing effects predominantly drive intermolecular interactions in complexes. Our approach involved utilizing density functional theory (DFT) calculations along with Bader's quantum theory of 'atoms-in-molecules' (QTAIM) to analyze electron density features such as charge density (ρ) and the Laplacian of charge density ($\nabla^2\rho$). Employing the properties of the electron density, we utilized recently developed Reduced Density Gradient (RDG)-based Noncovalent Interactions (NCI) index calculations for real-space visualization of both attractive interactions (van der Waals and hydrogen bonding) and repulsive interactions (steric).

The findings indicate the presence of noticeable C-H$\cdots\pi$ type interactions in this complex, as illustrated in Fig. S3.
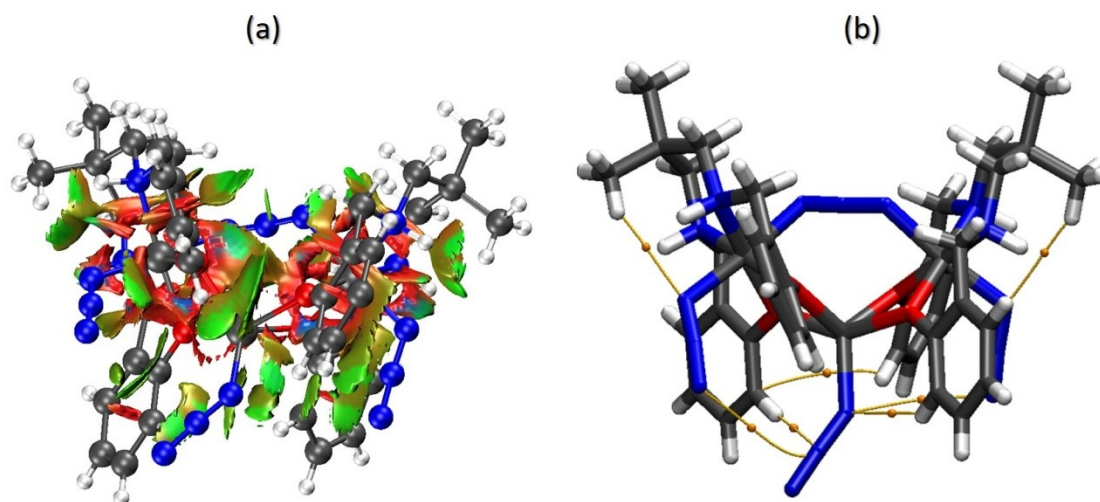

Fig. S5 (a) RDG-based NCI plot, and (b) AIM analysis for the investigated complex.

Band gap measurement from CV

Cyclic Voltammetry (CV) was employed to deduce the positions of valence band (V.B.) and conduction band (C.B.) of the material. Thereafter, the electrical bandgap, (ΔE) was determined by calculating the difference between energy levels of valence band, ($E_{V.B.}$) and conduction band, ($E_{C.B.}$) which provided the insights into the electronic properties of the material and also on how accurately the optical band gap was determined. Typically, the valence band level ($E_{V.B.}$) of a solid material is associated with its oxidation potential (E_{ox}) and the conduction band level ($E_{C.B.}$) is associated with its reduction potential (E_{red}) as given by the equations:

$$E_{V.B.} = - (E_{ox} + 4.8) \text{ eV}$$

$$E_{C.B.} = - (E_{red} + 4.8) \text{ eV}$$

$$\Delta E = (E_{C.B.} - E_{V.B.}) \quad \text{............ (I)}$$

The oxidation onset of the sample is at 1.69 V, corresponding to the valence band levels -5.83 eV and the conduction band levels at -3.22 eV which were calculated from their reduction onset at -0.92 V. Thus, the band gap of the sample was found to be 2.61 eV.

Device Fabrication

For the fabrication of metal-semiconductor Schottky device, Indium Tin Oxide (ITO) coated glass substrate was cleaned by acetone, distilled water, and isopropanol repeatedly and sequentially in ultrasonication bath for 10 min. At the same time, a well-dispersed solution of the cobalt based complex salt in N, N-dimethylsulfoxide (DMSO) medium was prepared followed by spin-coated onto the pre-cleaned ITO coated glass at 1000 rpm for 2 min employing SCU 2700 spin coating unit. Repetition of the spin coating step was continued for another 3 times. Thereafter, it was dried in a vacuum. The thickness of the film was measured

by the surface profiler and calculated around 1μm. The aluminium (Al) electrodes were deposited onto the film using the Vacuum Coating Unit (12A4D of HINDHIVAC) under a pressure of 10^{-6}Torr. The area of the Al electrodes was maintained as 7.065×10^{-6} m^2 with the help of the shadow mask. The measurements of current-voltage of the fabricated device employing the cobalt based complex salt was carried out by a Keithley 2635B source meter interfaced with PC under the dark and light condition in the voltage rangeof -1V to +1V at room temperature.
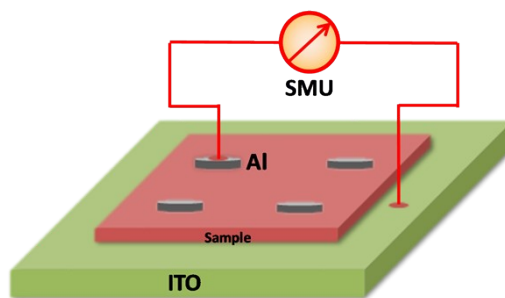

Fig. S6 The schematic diagram of the fabricated Schottky devices is given here. Here Al/material/ITO like structured device is fabricated. According to the picture four similar diodes have fabricated here at a time.

Here, we have also performed then temperature vs conductivity experiment with the fabricated Schottky diode. We have performed the experiment with four different temperatures (300 K, 315 K, 330 K and 345 K) and by increasing the temperature value the conductivity values have increased which also satisfies the semiconducting nature of the materials. The experimental data is given in Table S1.

Electrical Characterization

The Thermionic Emission (TE) theory is adopted to get more insights of the charge transport mechanism in the devices.[S12] The current of a diode can be expressed as the following equations according to TE theory.[S13]

$$I = I_0 \exp\left(\frac{qV}{\eta kT}\right)\left[1 - \exp\left(-\frac{qV}{\eta kT}\right)\right] \quad \ldots\ldots(II)$$

Where,

$$I_0 = AA^*T^2 \exp\left(-\frac{q\phi_B}{kT}\right) \quad \ldots\ldots(III)$$

$$\phi_B = \frac{kT}{q}\ln\left(\frac{AA^*T^2}{I_0}\right) \quad \ldots\ldots\ldots(IV)$$

Where, I_0 indicates the saturation current, q represents the electronic charge, k is the Boltzmann constant, T is the temperature in Kelvin, V is the forward bias voltage, η is the ideality factor, ϕ_B is the effective barrier height at zero bias, A is the diode area (7.065×10^{-6} m^2), A^* is the effective Richardson constant (1.20×10^6 $Am^{-2}K^{-2}$). From Cheung, the forward bias I-V characteristics in term of series resistance can be expressed as.[S14]

$$I = I_0 \exp\left[\frac{q(V - IR_S)}{\eta kT}\right] \quad \ldots\ldots. (V)$$

Where, the IR_S term represents the voltage drop across series resistance of device. In this circumstance, the values of the series resistance can be determined from following functions using equation (VII).[S15]

According to Cheung's model:

$$\frac{dV}{d\ln(J)} = \left(\frac{\eta kT}{q}\right) + R_S AJ \quad \ldots\ldots\ldots. (VI)$$

$$H(J) = R_S AJ + \eta\phi_B \quad \ldots\ldots\ldots(VII)$$

and H(J) can be expressed as:

$$H(J) = V - \left(\frac{\eta kT}{q}\right) \ln\left(\frac{J}{A^*T^2}\right) \qquad \text{............ (VIII)}$$
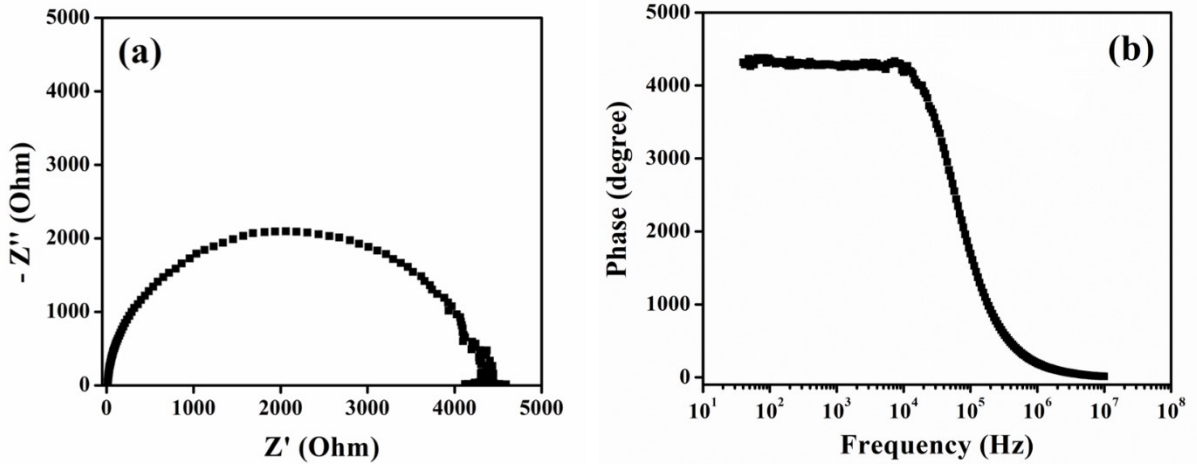
Nyquist plot and Bode plot

Fig. S7(a) Nyquist Plot and (b) Bode phase plot for the Al/sample/ITO Schottky barrier diode.

BVS calculation

The bond valence sum (BVS) method[S16-S20] has been performed to calculate the oxidation state of the metal ions in the solids based on crystallographically determined metal–ligand bond distances. The bond valences (S_{ij}) are calculated according to Eq. (IX).

$S_{ij} = \exp\left[(r_0 - r_{ij})/b\right]$ ....(IX)

where, i = donor centre; j = metal centre; r_0 = reported bond length between i and j; r_{ij} = the observed bond length, S_{ij} = the valence of a bond between two atoms i and j. and b is usually taken to be 0.37. Bond Valence Sum is finally calculated according to the Eq. (X), the valence sum rule (Pauling's second rule) is defined as

$Z_j = \Sigma S_{ij}$...............(X)

where, Zj is the valence of atom j connecting i-j bonds with all neighbouring i atoms. The bond valence sum (BVS) calculations have been performed to calculate the oxidation states of cobalt centers in the investigated complex. The BVS values for Co(1), Co(2) and Co(3) centers are respectively 2.121, 3.618 and 3.645(Table S2), are in good agreement for confirming the existence of trinuclear cobalt(III)-cobalt(II)-cobalt(III) in the said complex.

Table S1 Temperature vs Conductivity experiment of the investigated complex

Temperature (K)	Conductivity (Sm^{-1})
300	1.05×10^{-6} Sm^{-1}
315	1.19×10^{-6} Sm^{-1}
330	1.28×10^{-6} Sm^{-1}
345	1.39×10^{-6} Sm^{-1}

Table S2 Bond valence sum calculation and the related parameters for the complex

Metal centre	$i{-}j$ reported	r_0	$i{-}j$ of this complex	r_{ij}	s_{ij}	z_j
Co1	O$-$Co^{2+}	1.68	O(1)-Co(1)	2.020	0.399	2.121
	O$-$Co^{2+}	1.68	O(2)-Co(1)	2.099	0.322	
	O$-$Co^{2+}	1.68	O(3)-Co(1)	2.087	0.333	
	O$-$Co^{2+}	1.68	O(4)-Co(1)	2.013	0.406	
	N$-$Co^{2+}	1.80	N(8)-Co(1)	1.953	0.661	
Co2	O$-$Co^{2+}	1.68	O(1)-Co(2)	1.897	0.556	3.618
	O$-$Co^{2+}	1.68	O(2)-Co(2)	1.943	0.491	
	N$-$Co^{2+}	1.80	N(1)-Co(2)	1.979	0.616	
	N$-$Co^{2+}	1.80	N(2)$-$Co(2)	1.976	0.621	
	N$-$Co^{2+}	1.80	N(5)$-$Co(2)	1.998	0.585	
	N$-$Co^{2+}	1.80	N(11)$-$Co(2)	1.907	0.749	
Co3	O$-$Co^{2+}	1.68	O(3)-Co(3)	1.902	0.549	3.645
	O$-$Co^{2+}	1.68	O(4)-Co(3)	1.922	0.519	
	N$-$Co^{2+}	1.80	N(3)-Co(3)	1.980	0.615	
	N$-$Co^{2+}	1.80	N(4)$-$Co(3)	1.980	0.615	
	N$-$Co^{2+}	1.80	N(7)$-$Co(3)	1.989	0.600	
	N$-$Co^{2+}	1.80	N(14)$-$Co(3)	1.908	0.747	

Table S3 Mulliken Spin population and atomic charge of the investigated complex

Atom	Alpha pop	Beta pop.	Spin pop.	Atomic charge
Co(3)	8.25349	8.24307	0.01043	0.50344
Co(1)	9.51324	6.83402	2.67922	0.65274
Co(2)	8.25074	8.23897	0.01177	0.51030

References

S1 G. M. Sheldrick, *SHELXT. ActaCryst*, 2015, **71A**, 3–8.

S2 G.M. Sheldrick, SADABS, V2014/5, Software for Empirical Absorption Correction, University of Gottingen, Institute fur AnorganischeChemiederUniversitat, Gottingen, Germany, 1999–2003.

S3 S. K. Wolff, D. J. Grimwood, J. J. McKinnon, D. Jayatilaka, M. A. Spackman, Crystal Explorer 2.0, University of Western Australia, Perth, Australia, **2007**. http://hirshfeldsurfacenet.blogspot.com.

S4 M. A. Spackman and D. Jayatilaka, *CrystEngComm*, 2009,**11**, 19–32.

S5 F. L. Hirshfeld, *Theor. Chim. Acta*, 1977,**44**, 129–138.

S6 H. F. Clausen, M. S. Chevallier, M. A. Spackman and B. B. Iversen, *New J. Chem.*,2010, **34**, 193–199.

S7 A. L. Rohl, M. Moret, W. Kaminsky, K. Claborn, J. J. McKinnon and B. Kahr, *Cryst. Growth Des.*, 2008,**8**, 4517–4525.

S8 A. Parkin, G. Barr, W. Dong, C. J. Gilmore, D. Jayatilaka, J. J. McKinnon, M. A. Spackman and C. C. Wilson, *CrystEngComm*,2007, **9**, 648–652.

S9 M. A. Spackman and J. J. McKinnon, *CrystEngComm*,2002, **4**, 378–392.

S10 F. H. Allen, O. Kennard, D. G. Watson, L. Brammer, A. G. Orpen and R. J. Taylor, *J. Chem. Soc. Perkin Trans.*, 1987, **2**, S1–S19.

S11 J. J. Kinnon, M. A. Spackman and A. S. Mitchell, *Acta Cryst.*, 2004, **B60**, 627–668.

S12 E. H. Rhoderick and R. H. Williams, Metal-Semiconductor Contacts, Clarendon Press, Oxford, 2nd edn, **1988**.

S13 S. M. Sze, Physics of Semiconductor Devices, Wiley, New York., **1981**.

S14 S. Sil, R. Jana, A. Biswas, D. Das, A. Dey, J. Datta, D. Sanyal and P. P. Ray, IEEE Trans. Electron Devices, 2020, **67**, 2082–2087.

S15 M. Das, J. Datta, A. Dey, R. Jana, A. Layek, S. Middya and P. P. Ray, *RSC Adv.*, 2015, **5**, 101582–101592.

S16 N.E. Brese and M. O'Keeffe, *Acta Crystallogr. B*, 1991, **47**, 192–197.

S17 I.D. Brown and D. Altermatt, *Acta Crystallogr. B*, 1985, **41**, 244–247.

S18 M. O'Keeffe and N.E. Brese, *J. Am. Chem. Soc.*, 1991, **113**, 3226–3229.

S19 H.H. Thorp, *Inorg. Chem.*, 1992, **31**, 1585–1588.

S20 G. J. Palenik, *Inorg. Chem.*, 1997, **36**, 122.